THE ROLE OF BACKGROUND CLOUD MICROPHYSICS IN SHIP TRACK FORMATION

S. PLATNICK[1], P. A. DURKEE[2], K. NIELSON[2], J. P. TAYLOR[3], J. A. COAKLEY[4]

S-C. TSAY[5], M. D. KING[5], R. J. FEREK[6], P. V. HOBBS[6]

[1] NASA Goddard Space Flight Center, Greenbelt, Maryland
and University of Maryland Baltimore County

[2] Naval Postgraduate School, Monterey, California

[3] U.K. Meteorological Research Flight, Farnborough, U.K.

[4] Oregon State University, Corvalis, Oregon

[5] NASA Goddard Space Flight Center, Greenbelt, Maryland

[6] University of Washington, Seattle, Washington

to be submitted to JAS

Monterey Area Ship Track Experiment special issue

May 1996

ABSTRACT

We investigate the extent to which the brightness of ship tracks observed in visible and near-infrared imagery can be explained by the microphysics of the background cloud in which they form. The paper begins with a quantification for the meaning of track formation. A track's contrast brightness, i.e., the relative reflectance change, is used as such a measure. The sensitivity of visible and near-infrared wavelengths for detecting reflectance changes in ship tracks is discussed, including the use of a modified cloud susceptibility parameter for accessing the sensitivity of background microphysics on potential track development. It is shown that the relative change in cloud reflectance for ship tracks is expected to be larger in the near-infrared than in the visible and that 3.7μm channels, widely known to be useful for detecting tracks, can be demonstrated to have the greatest sensitivity. Retrievals of cloud microphysics and optical thickness have been made with the high spatial resolution (50m at nadir, 35km swath width) MODIS Airborne Simulator (MAS) flown on NASA's high altitude ER-2 aircraft and with the larger scale perspective of the Advanced Very High Resolution Radiometer (AVHRR). Observed modifications in cloud droplet effective radius, optical thickness, and liquid water path are presented for several ship tracks formed in background clouds with both small and large droplet sizes. Results are used to test the use of the susceptibility parameters in predicting ship track formation from background cloud parameters. The remote sensing retrievals are augmented with in situ measurement of cloud microphysics and cloud reflectance from the UK Meteorological Research Flight C130 aircraft providing data at the smallest spatial scales.

1. Introduction

Ship tracks have provided intriguing examples of cloud albedo modification by anthropogenic aerosols since their discovery with early satellites by Conover (1966) and their proposed explanation by Conover (1966, 1969) and Twomey et al. (1968). Discussion of a possible climatic consequence to large-scale aerosol pollution modification of cloud albedo by Twomey (1974, 1977) gave the ship track phenomena considerable attention in cloud-climate interaction studies (e.g., Charlson et al. 1992). Though ship tracks certainly provide a possible microcosm for this so-called *indirect effect* of aerosols on climate, their interest in this paper is from a local perspective only. Ship tracks are interesting in their own right, in addition to providing one of the best instances of a *control* cloud for use in cloud microphysical and radiative studies. That is, a track can be expected to develop in conditions identical to the background cloud in which it forms, with the probable exception of the modification to a single input – the aerosol amount.

The Monterey Area Ship Track Experiment (MAST) provided a unique opportunity for the remote sensing of ship tracks and the background marine stratocumulus in which they form. Using imagery and in situ data acquired during the MAST experiment, this paper first explores the extent to which the existence of ship tracks, specifically, their detection with multispectral imagery, can be explained by parameters of the background cloud. These parameters include droplet size, liquid water content, and optical thickness. Depending on the wavelength, the droplet size and/or optical thickness of the background cloud will be shown to be the crucial parameters. Secondly, we

ask whether the relative brightness of a track can be correlated with the background cloud parameters. That is, to what extent can the strength, or *contrast*, of observed tracks be predicted from knowledge of microphysics and optical thickness in the surrounding cloud alone. The following sections explore the radiative implications of track detection and track contrast. Taken together, these two aspects are considered to define a track's radiative *formation* as used in the title.

Clearly, the resulting increase in cloud droplet numbers caused by the ship plays a fundamental role in track brightness, in addition to background cloud conditions. This will be discussed in more detail later. It is also understood that there are meteorological conditions that need to be met for the development of tracks just as there are for the background cloud. Further, dynamics could perhaps dictate that the track will develop in ways different than unaffected parts of the cloud. These dynamic influences are the subject of other papers in this special issue. In the following discussions, we deal only with the cloud microphysical component.

The background cloud parameters needed for the analysis are mostly obtained with remote sensing cloud algorithms applied to multispectral imagery, though some in situ measurements are also used. Retrieval of cloud droplet size, optical thickness, and liquid water path is inferred from solar reflection measurements in the visible and near-infrared which are non-absorbing and absorbing, respectively, for cloud droplets. As a simplification, the visible reflectance primarily contains the optical thickness information while the near-infrared reflectances indicate size since absorption is approximately proportional to droplet radius. The typical absorbing channels, dictated by the atmospheric windows, are in the 1.6μm,

2.2μm, and 3.7μm bands. The 3.7μm band posses additional difficulty in that cloud emission is a significant part of the total measured radiance and must be removed. This study uses two imaging radiometers: the Moderate Resolution Imaging Spectroradiometer (MODIS) Airborne Simulator (MAS) flown on NASA's high-altitude ER-2 aircraft (King et al. 1996), and the Advanced Very High Resolution Radiometer (AVHRR) onboard the National Oceanic and Atmospheric Administration (NOAA) polar-orbiting satellites. The MAS contains spectral channels in all the visible and near-infrared bands useful for cloud remote sensing. On the AVHRR, the sole droplet absorption channel for solar radiation is at 3.7μm. At nominal ER-2 altitudes of 20km, the MAS nadir resolution for marine boundary layer clouds is 50m with a swath width of 35km. The high spatial resolution offers an unprecedented view of ship track structure. The ER-2 made seven flights during MAST; ship tracks were found in MAS imagery on three of the flight days. AVHRR 1km data was acquired by the Naval Postgraduate School in Monterey, California. While having much less spatial resolution than the MAS, AVHRR instruments provided multiple daily passes of the MAST operations area and are capable of larger scale studies with their 2400km swath width. This paper will look at track retrievals from six morning passes of NOAA-12. The U.K. Meteorological Research Flight C130 aircraft provided in situ droplet radius and above cloud reflectance measurements. This data provide the highest spatial resolution but with limited spatial sampling. Measurements from all three platforms are useful for developing ship track microphysical statistics and in accessing the correlation between near-infrared susceptibilities and track strength.

Section 2 begins with a review of the physics behind the reflectance

increases, both visible and near-infrared, observed in ship track imagery. The increase in droplet numbers expected in ship tracks is expected to result in both an increase in cloud optical thickness and a decrease in droplet sizes, the latter increasing visible reflectance and the former dominating near-infrared increases in reflectance as droplet absorption decreases. The sensitivity of relative reflectance changes to modification in droplet numbers is discussed in terms of a cloud susceptibility parameter. It will be shown that sensitivities increase with increasing absorption, or wavelength, with the 3.7μm sensitivities being the largest and typically several factors greater than in the visible (as noted in the AVHRR work of Scorer 1987; Coakley et al. 1987). Section 3 presents results of MAS and AVHRR retrievals including some statistics of droplet size, optical thickness and liquid water path changes. Finally, the utility of using background microphysics in predicting ship track brightness with near-infrared susceptibilities is discussed in section 4.

2. The sensitivity of the visible and near-infrared in ship track detection

A. Cloud reflectance in the visible and near-infrared

Bidirectional reflectance of solar radiation from clouds depends fundamentally on a combination of the cloud's optical thickness, τ, the cloud droplet single scattering albedo, ϖ_o, and the droplet scattering phase function. For a given set of microphysical conditions, optical thickness has a wavelength dependence through the extinction efficiency. The single scattering albedo is the fraction of energy scattered by a droplet and so

fractional absorption is given by $1-\varpi_o$. Absorption of liquid water is negligible in the visible and $\varpi_o=1$. In the near-infrared where liquid water absorption is significant, droplet absorption is approximately proportional to the product of droplet radius and water bulk absorption at the wavelength of interest (Twomey and Bohren 1980; Stephens and Tsay 1990). That is, at any given wavelength, larger droplets tend to absorb more radiation than smaller ones. Likewise, clouds with larger droplets reflect less energy. This has significant implications for ship tracks observations and the remote sensing of droplet sizes. For multiple scattering situations such as in the clouds of this study, the effect of the phase function can often be described by the asymmetry parameter, g, a scalar representing the average energy scattered into the forward direction (varying from about 0.8 to 0.9 for droplets in the visible and near-infrared). As with single scattering albedo , the asymmetry parameter also depends on droplet size and wavelength. In general, the larger the droplet the larger the asymmetry parameter and the more forward scattering. With more forward scattering there is less chance of incoming photons being turned around and cloud reflectance decreases. In summary, for a fixed cloud optical thickness, as droplet sizes increase both absorption and forward scattering increase and cloud reflectance decreases. Of the two influences, absorption greatly dominates the scattering effect. For fixed droplet sizes, reflectance will increase with optical thickness though with diminishing importance into the near-infrared. Both decreases in droplet size and increases in optical thickness are expected in ship tracks when liquid water content remains constant.

For a distribution of droplet sizes, as occurs in clouds, the droplet effective radius, r_e, is the pertinent radiative transfer size parameter (defined as

$\langle r^3 \rangle / \langle r^2 \rangle$). Therefore, we can now write the functional dependence of reflectance as $R=R_\lambda(\tau,\varpi_o,g)=R_\lambda(\tau,r_e)$. These concepts are summarized in Fig. 1 which shows the calculated reflectance for a plane-parallel cloud as a function of optical thickness. The various curves cover the visible and near-infrared bands used in the MAS and AVHRR instruments and three different effective radii. In the near-infrared, liquid water absorption increases with increasing wavelength and so reflectance curves for the same droplet size are seen to decrease significantly at the longer wavelengths. Likewise, for a fixed band, reflectance decreases with increasing droplet sizes as absorption increases. In the visible it is the relatively small effect of asymmetry parameter which accounts for the slight decrease in reflectance for the larger droplets. For a given absorption, or droplet size, reflectance is seen to eventually reach an asymptotic limit as optical thickness increases to a point where photons can no longer survive the many scatterings it takes to reach the bottom of the cloud and then return to cloud-top. From a remote sensing standpoint, it is clear that reflection measurements in both the visible and near-infrared contain information about both optical thickness and droplet effective radius. The most unambiguous information occurs when the near-infrared reflectance has reached its asymptotic value and is no longer dependent on the retrieval of optical thickness. For the present purpose, it is also clear that changes in cloud droplet sizes can be observed as changes in near-infrared reflectance.

B. Visible and near-infrared cloud susceptibilities

The need to adopt a definition of what constitutes a ship track is an

obvious first step in an investigation on their formation. That is, a detection criteria with which a track is said to exist is necessary. Previous studies with 3.7μm imagery makes it an obvious choice. In this section, we explore the sensitivity of all near-infrared imagery, including the 3.7μm band, for track detection. Further, it will be shown that 3.7μm imagery is likely to be much more sensitive a method for detecting microphysical changes than current in situ instrumentation. If a track is defined by a noticeable increase in reflectance, then detectability means that the relative change in the reflectance, i.e., $\Delta R/R$, or track contrast, is larger than instrument noise and existing cloud variability. The influence of background cloud parameters on ship track development then becomes a measure of its influence on potential $\Delta R/R$.

A ship is believed to modify droplet concentrations, N, by contributing cloud condensation nuclei into the developing or existing cloud (Conover 1966; Twomey et al. 1968). One measure for the sensitivity of cloud albedo to changes in cloud droplet concentration is dA/dN which has been defined as *cloud susceptibility* (Twomey 1991, Platnick and Twomey 1994), where A is cloud albedo. Intended as a sensitivity parameter for indicating the potential indirect effect of aerosol on climate, it can also be used for present purposes with slight modification. In the context of this paper, an indicator of potential ship track formation would be $(dR/R)/dN$ where it is the relative change in bidirectional reflectance as seen from satellite or airborne platforms that is the appropriate quantity. This can be termed a *contrast susceptibility* to distinguish it from the original definition of cloud susceptibility. Unless noted, further use of the term susceptibility will refer to the contrast formulation. Recalling that reflectance for a particular band has the

functional dependence $R(\tau,r_e)$, the derivative can be written as

$$\frac{1}{R}\frac{dR}{dN} = \frac{1}{R}\left(\frac{\partial R}{\partial r_e}\frac{dr_e}{dN} + \frac{\partial R}{\partial \tau}\frac{d\tau}{dN}\right), \quad (1)$$

where the wavelength dependence is understood. With the assumption that the liquid water content, W, in tracks remains the same as in the background cloud, ship track optical thickness would be expected to increase above the background value by $N^{1/3}$ and droplet sizes would decrease as $N^{-1/3}$. Results from remote sensing retrievals presented in the next section, do not suggest that liquid water content in a track is, on average, significantly increased compared with the background cloud as was suggested by the measurements of Radke et al. (1989). For such a constant liquid water process, contrast susceptibility can be written as

$$\frac{1}{R}\frac{dR}{dN} = \frac{1}{R}\frac{C}{W}\left(-\frac{\partial R}{\partial r_e}r_e^4 + \tau\frac{\partial R}{\partial \tau}r_e^3\right) \quad (2)$$

where the constant $C = 4\pi\rho_l/9$ with ρ_l as the density of liquid water. In the visible, the second term dominates while for the 3.7μm band, the second term vanishes (cf. Fig. 1). Note that $\partial R/\partial r_e$ is a negative quantity ensuring that near-infrared reflectance increases with droplet concentration. A detailed derivation of Equ. 2 is not given as it closely follows the development of cloud susceptibility in Platnick and Twomey (1994), including assumptions

regarding the relationship between various moments of the droplet size distribution (also see Taylor and McHaffie 1994). Figure 2a shows contrast susceptibility calculated as a function of effective radius in visible and near-infrared bands for an optical thickness of 20. It is seen that the susceptibility increases with the longer wavelengths as the droplet absorption effect dominates. Figure 2b gives the ratio of the 3.7μm contrast susceptibility to the visible for a range of optical thicknesses. The sensitivity in the 3.7μm band is shown to be a factor of two to eight greater than in the visible for the prescribed geometry. The partial derivatives are determined from model calculations of reflectance. However, approximations are useful for instructive purposes. For example, neglecting the droplet size dependence of the asymmetry parameter, two-stream approximations for the visible reflectance (Bohren 1980) can be used to write $\tau\partial R/\partial\tau$ in the second term of Equ. 2 as *R(1-R)*, giving the optical thickness dependence of the equation as

$$\frac{1}{R_{vis}}\frac{dR_{vis}}{dN} \approx \frac{C}{W}(1-R_{vis})\,r_e^3. \tag{3}$$

A fitting routine applied to Fig. 1 finds that for effective radii between 5μm and 20μm and a wide range of solar angles, the 3.7μm reflectance can be approximate by the power law $R_{3.7} \approx 2.9 r_e^{-1.2}$. If a power law can adequately describe reflectance then it can be shown that, regardless of the value of the exponent, $R_{3.7}^{-1}\left(R_{3.7}/\partial r_e\right) \propto r_e^{-1}$. Substituting the approximation into Equ. 2 gives

$$\frac{1}{R_{3.7}}\frac{dR_{3.7}}{dN} \approx 1.2 \frac{C}{W} r_e^3. \quad (4)$$

For example, with W=0.3gm^{-3}, Equ. (4) becomes $\approx 5.7x10^{-6} r_e^3$, with r_e in microns and contrast susceptibility in cm^3. With r_e=12μm, the susceptibility would be about 0.01cm^3 implying that a 3.7μm channel contrast of 1% would result from an increase in droplet concentration of only 1cm^{-3}. Note that the approximations of Equs. 3 and 4 both have an r_e^3 dependence. The ratio of the 3.7μm to visible susceptibility is approximated as simply $1.2/(1-R_{vis})$ which is a constant for any prescribed optical thickness (or R_{vis}) and in good agreement with Fig. 2b for the larger effective radii. All calculations of susceptibility in the following sections use a nominal liquid water content of 0.3gm^{-3}.

Figure 2 indicates that, from radiative considerations alone, ship tracks are expected to be more easily observed in the near-infrared channels then in the visible, and that the 3.7μm channel has the most sensitivity (noticed in the observations of Coakley et al. 1987). Though the plots of Fig. 2 are for differential changes in droplet numbers, large differences in droplet sizes are fairly well approximated by the same curves. An example of contrast is seen in the four-channel MAS images of Fig. 3 for two tracks, both of which formed in relatively clean background conditions. Retrievals for these tracks are discussed in the next section. However, for present purposes, we note that the apparent track contrast become more obvious as the channel wavelength increases. For the relatively high sun angles in these images (cosine of the solar zenith angle about 0.95), track contrast in the 3.7μm channel is only expected to be about a factor of 1.6 greater than for the visible channel. AVHRR images have lower sun angles present at these latitudes during the

satellite overpass and contrast differences should be more dramatic as indicated by Fig 2. In addition to contrast depending on wavelength according to the simple model outlined above, it is also seen that background variability in the visible image of 29 June 1994 appears to be obscuring the track and reducing contrast. The effect of optical thickness variability on track contrast was discussed by Coakley et al (1987).

As a measure of the channel's ability to detect non-differential microphysical changes, Fig. 4 shows the 3.7μm relative reflectance change that accompanies a given decrease in track effective radius. It is seen that sub-micron changes in droplet sizes can easily be observed. For example, a relative reflectance increase of 5%, which should be obvious in most sensors for correspondingly small background variability, would indicate a reduction in droplet size of only 0.5μm. Such sensitivity is likely to be larger than commonly used in situ instruments such as the Forward Scattering Spectrometer Probe (FSSP) with its 3μm droplet size bins (Knollenberg 1981), especially against the natural variability seen in aircraft data (Ferek et al. 1996). However, since 3.7μm imagery includes a significant thermal component, it should be noted that a relative reflectance increase of 5% would mean a smaller increase in the total measured channel radiance. If a track does not significantly alter the thermal emission component, the relative change in total observed channel radiance, I_R+I_E, would be $(\Delta R/R)(1+I_E/I_R)^{-1}$ where I_E is the emitted radiance, or intensity, and I_R is the reflected radiance. Radiative transfer calculations suggest that $1+I_E/I_R$ can be approximated as a linear function of effective radius. For example, with cloud-top temperatures of 285K (reasonable for the clouds of this study) and optically thick clouds, $1+I_E/I_R \approx 0.7+0.085r_e$ with r_e in microns. Using this approximation for the

above example, a 5% increase in relative reflectance would correspond to an increase in measured radiance of about 3% for an effective radius of 10μm, still within sensor capability. The linear approximation ranges from $0.8+0.06r_e$ to $0.6+0.13r_e$ for cloud-top temperature of 275K to 290K, respectively, with the geometry given in Fig. 1.

The above discussion was focused mainly on the detectability of ship tracks in multi-wavelength imagery. A second goal of this paper is to understand the role of cloud microphysics in the observed contrast of ship tracks. In addition to knowledge of the background cloud's droplet size, optical thickness, and liquid water content (collectively represented by the contrast susceptibility parameter), a prediction of droplet concentration changes, ΔN , is needed to infer ship contrast. For small changes in either ΔN or $\Delta N/N$, track contrast is approximately the product of contrast susceptibility and the droplet concentration change. Figure 5a shows plots of track contrast versus susceptibility for a wide range of ΔN. Figure 5b shows the same plot versus effective radius where the r_e^3 dependence of susceptibility is seen. A liquid water content of $0.3 gm^{-3}$ is used in the calculations and solar and viewing angles are the same as in Fig. 1. Smaller liquid water contents will shift the curves to the right, such that a given susceptibility will correspond to a smaller contrast for the same ΔN. There is some angular dependence as well. Figure 5 *is* the role of background cloud microphysics in track formation – the abscissa parameterizes microphysics and the ordinate is the measure of formation. The range of observed ΔN in actual ship tracks is important in determining the effect to which a set of curves like those of Fig. 5 are useful in approximating ship contrast from susceptibility alone. Two possibilities come to mind. If measured in situ droplet increases are typically found to be within

some reasonable bounds then such empirical information could be used to determine the uncertainty in inferring track contrast from the figure. **[? For instance, though aerosol and cloud condensation nuclei numbers may be very large in tracks, droplet numbers typically show a more moderate range of increases. Further, measurements of droplet increases by the University of Washington C-131A did not show dramatic differences between clean or polluted air, indicating a limiting influence on droplet activation (refs. this issue). ?]** Secondly, if droplet increase is found to depend to some extent on background microphysics, which is described by susceptibility, then the broad range in track contrast covered by the multiple curves of Fig. 5 should be reduced. Several papers in this volume should be helpful in addressing these issues (refs. this issue).

Contrast susceptibility represents the radiative role of microphysics in track formation using a simple model for the cloud droplet interactions including conserved liquid water content and vertical homogeneity. It would be expected that this simple description might not always be successful in describing track formation.

3. Remote sensing results

A. MODIS Airborne Simulator results

Though the current MAS data system allows for the recording of 50 channels (King et al. 1996) from the visible through the thermal infrared, during the MAST experiment in June 1994, the MAS data system was limited

to 11 spectral channels. Channels were chosen in those bands most useful for cloud remote sensing. Specifically, center wavelengths of channels selected for the MAST configuration were at: 0.65μm, 0.87μm, 1.62μm, 1.89μm, 2.13μm, 2.29μm, 3.74μm, 3.90μm, 8.60μm, 11.02μm, and 11.98μm. All channels were recorded at 8 bits with the exception of the 3.7μm and thermal channels which were recorded at 10 bits. Seven ER-2 flights were made during MAST covering an region as far as 500 km off the coast of Monterey Bay. Flight plans typically involved offset parallel runs to map out large regions and increase the chances of overflying a track. For logistical reasons, flights were flown during midday. Tracks were found in MAS imagery on 13 June, 29 June, and 30 June 1994. Background cloud droplet sizes were relatively large on 13 June and 29 June while relatively small droplets were found in the clouds of 30 June.

The cloud retrieval algorithm using a 3.7μm band for the absorbing channel is discussed in detail in Platnick and Valero, 1995; retrievals using shorter wavelengths are special (simpler) cases of this algorithm. As previously discussed, a combination of visible and near-infrared channels are necessary to retrieve optical thickness and droplet size. The choice of the near-infrared channel depends to some extent on the application of the retrieval. For instance, stratocumulus boundary layer clouds are known to have measurable increases of both droplet sizes and liquid water content with height (e.g., Noonkester 1984; Garrett and Hobbs 1995). Retrievals of droplet size using any of the near-infrared channels will be weighted towards the upper part of the cloud. For example, consider a cloud with optical thickness 10, effective radius equal to 10μm, and the cosine of the solar zenith angle, μ_o, equal to 0.65. Then average reflected photons in the 1.6μm, 2.2 μm, and 3.7μm

MAS channels are found to penetrate to an average optical depth of 3.5, 3.1, and 1.5, respectively. Less absorption gives greater weighting to droplet sizes farther down in the cloud. None of the channels can provide exact liquid water paths (LWP) which is approximated from the retrievals as $2\tau r_e/3$, with r_e in microns, but is actually a vertical integration of that product. However, the 2.2μm retrieval with its deeper weighting might be expected to provide better estimates than the 3.7μm channel. The 1.6μm channel may also be useful for this purpose, though it's solution is more sensitive to optical thickness (cf. Fig. 1). The 1.6μm retrievals agree well with the 2.2μm and both are consistent with droplet size profiles measured from the University of Washington C-131A FSSP-100 which underflew the MAS on most ER-2 flights. The 3.7μm retrievals are generally 2-4μm larger than expected from the cloud-top measurements. It is not obvious whether this discrepancy indicates error in the physical theory, cloud model, imager and/or in situ instrument characterization, atmospheric effects, or perhaps all of the above (a discussion of error sources and validations for this band can be found in Platnick and Valero 1995 and Han et al. 1995).

The 2.2μm retrievals are shown in this section because of agreement with in situ measurements and the likelihood of being more representative of the vertically integrated liquid water path. Susceptibilities based on MAS retrievals in the final section will use the 3.7μm channel. This is because the channel's reflectance is a fundamental part of the calculation suggesting that model estimations should be avoided if possible, especially if error in physical theory or model is a possible component to the retrieval discrepancy. In the 3.7μm channel, high sun angles caused enhanced glory reflectances to cover part of the imaged clouds on most days. In these glory regions, significant

changes in reflectance can occur over small MAS scan angles as the details of the scattering phase function are seen in single scattered photons in backscattered directions (cf. Nakajima and Spinhirne 1994). The default reflectance and emittance libraries used in the retrievals have angular intervals equivalent to $\Delta\mu$=0.1 for both solar and satellite zenith angles (Platnick and Valero 1995). The angular resolution needed in the libraries to account for glory directions at all possible scattering geometries would result in much larger libraries where resolution on the order of a few degrees would be needed. Normally, these glory viewing angles could be avoided in the 3.7μm retrievals. When glory directions could not be avoided, a modified library was used where the single scattering component as calculated by an adding/doubling code (Twomey 1966) at the angular intervals of $\Delta\mu$=0.1 had been removed. Then the exact phase function, using precise scattering angles, was used to account for the single scattering component of reflectance and added to an interpolated library value. A thermal infrared channel is used to estimate cloud top temperature for removing 3.7μm channel emission. The correlated k-distribution technique of Kratz (1995) was used to calculate atmospheric transmission and/or emission for all MAS and AVHRR channels. Atmospheric water vapor and temperature profiles needed for the calculations were taken from sondes released from the ship Glorita (ref.) during MAST.

Figure 6 shows retrieval results for the southern portion of the Star Livorno ship track on 29 June 1994 which formed in a clean boundary layer (Ferek et al. 1996). The MAS shows a surprising complex scene at this high spatial resolution. The images cover an area of about 35km along an instrument scan line (the horizontal dimension on the figure) by 70km in the

vertical; pixels have not been spacially re-sampled across the scan line. The track width is about 7km at the center of the images. The background cloud is seen in the figure to have relatively large, and highly variable, droplet sizes and a roll-cloud structure with some open areas. In situ microphysical measurements by the University of Washington C-131A showed the same similar variability (Ferek et al. 1996). Retrieved in-track effective radii are smaller than background sizes by about 5μm or more. Background cloud optical thickness is also quite variable and might be partially responsible for obscuring the track in the optical thickness retrieval (see also Fig. 3). However there are many small-scale locations where a substantial decrease in droplet size corresponds to no significant change in the optical thickness. Since ship track optical thickness does not obviously change with respect to nearby background thicknesses, liquid water path merely follows the reduction in droplet sizes seen in the effective radius retrievals. An unidentified ship track formed on 30 June 1994 in a relatively uniform, thick, background cloud with small droplet sizes as shown in Fig. 7. The imaged region is about 35km in the horizontal dimension by 40km in the vertical. The track was seen in several adjacent ER-2 flight legs and is about 9km wide. In-track effective radius shows a fair amount of structure along the edges, but has well-defined minima. Both background and in-track optical thickness are large and variable. Again, ship track optical thickness is not greatly modified from the background cloud resulting in inferred decreases in track liquid water path in most track regions as shown in the last panel of the figure. The variability seen in Figs. 6 and 7 suggest that track statistics derived from aircraft or surface ships could easily be biased by insufficient sampling. Figure 8 serves to summarize MAS retrievals with histograms for selected regions of Figs. 6 and

7 and several locations along the unknown ship track of 13 June 1994 shown in Fig. 3. Droplet size reductions are significant in all cases while optical thickness increases are small and generally within the background cloud variability (with the possible exception of the 13 June track).

B. AVHRR results

Multiple tracks, extending over large regions, were found on 12, 13 14, 27, 28, and 29 June 1994 in NOAA-12 imagery collect by the Naval Postgraduate School. For these six days, more than 18,000 pairs of in-track and nearby background cloud samples were collected from a total of about 110 tracks. Histograms of changes in cloud parameters for two of the days are shown in Fig. 9. As with the MAS retrievals, droplet size changes are most obvious, optical thicknesses are slightly increased on average, and resulting estimates of liquid water path show a slight decrease on average. The AVHRR retrievals gave significantly higher occurrences of large droplets (>15-20μm) than MAS retrievals. With larger pixel sizes, it is possible that these retrievals could suffer from inclusion of pixels which are not completely cloud filled. An attempt was made to screen such pixels by averaging over small areas and only using pixels with thermal radiances below some specified value for calculation of the individual samples. The issue of cloud fraction in these 1km pixels is of critical importance. Calculations suggest that cloud-filled fractions of 0.7, for example, could increase retrieved effective radii by 4-6μm over actual values while retrieved optical thicknesses would decrease. It is not clear whether cloud fraction would be different between track and background regions.

There is little pre-MAST ship track data with which to compare these retrievals. The in situ measurements of Radke et al. (1989) showed increases in liquid water content in the track they sampled. The AVHRR ship track retrievals of Platnick and Twomey (1994) mostly showed increases in liquid water path for a small sample of tracks on a single day in a region off the coast of Washington State; effective radius changes were significant and optical thicknesses generally increased. The retrievals of this study suggest that average increases in track optical thickness are often on the order of the background cloud variability though droplet size changes are obvious and can be quite large. Estimates of track liquid water path have shown a tendency to decrease relative to background values, especially in the limited number of MAS retrievals.

4. Background microphysics as a predictor of ship tracks

A summary of all AVHRR retrievals plotted as ship track contrast versus contrast susceptibility is shown in Figure 10. Averages for individual tracks are also shown. With the exception of data from 12 June 1994, the largest relative increases in track reflectance correspond to the larger susceptibilities. However, the great variability seen in all plots makes this relation less than definitive. Track-averaged points also show this variability.

Figure 11 shows a similar summary for MAS retrievals, which includes the three tracks from 13 June, 29 June, and 30 June 1994 discussed in the last section. The figure uses retrievals compiled for the regions displayed in the histograms of Fig. 8. Three additional tracks from 13 June 1994 are plotted

along with retrievals from 11 June 1994, a day of relatively uniform stratus in which no tracks were observed in the MAS imagery. Average values indicate a good correlation between track contrast and susceptibility. The standard deviations for these points, indicated by the bars, are seen to be fairly large. The deviation in the calculated contrast susceptibility is caused by variability in the retrieved effective radii of the background cloud. It increases for the larger susceptibilities because of the radius-cubed dependence. The standard deviation in track contrast is also affected by the size retrievals since droplet absorption, and therefore cloud reflectance and emission, vary with effective radius. For example, given the same measured 3.7μm radiance, a larger size retrieval would infer a larger cloud emission component and a smaller cloud reflectance. This deviation depends on both background and in-track size variability. One possible interpretation of the standard deviations is their consequence to sampling size. If variations from the average values are not random from pixel to pixel but indicate actual cloud variability which might exist on several scales, then large sampling sizes might be needed to give appropriate averages. For example, aircraft or ship measurements at limited locations in these track regions might only expect to be sampling somewhere within the standard deviation bars. The variability seen in the MAS retrievals of Figs. 6 and 7 makes these sampling concerns evident.

If average liquid water content is known, a set of curves similar to Fig. 5a can be overlaid on Fig. 11 to test the agreement to which observed contrast and susceptibility is consistent with droplet increases (ΔN). University of Washington C-131A in situ measurements of liquid water content on 29 June and 30 June 1994 were used to create such a set of curves. Since susceptibility results have been calculated for a nominal liquid water content of 0.3gm^{-3}, the

abscissa must be scaled by $0.3/W_{meas}$, where W_{meas} is the measured liquid water content, before a comparison can be made. The locations of the 29 June and 30 June averages imply droplet increases of about $40cm^{-3}$ for either day, while the C-131A measured increases of roughly $150cm^{-3}$ on both days (ref. special issue). This lack of consistency might be partially due to the 3.7μm droplet size retrievals being larger than in situ values as discussed in the previous section. Smaller effective radii would move points on Fig. 11 upward and to the left implying larger increases in droplet numbers (cf. Fig. 5) and better agreement with C-131A data. The discrepancy might also result from the simplicity of the susceptibility model.

The U.K. Meteorological Research Flight C130 aircraft made in situ cloud microphysical measurements and above-cloud reflectance measurements during MAST. Effective radius derived from combined FSSP and 2-DC droplet spectra (see Martin et al. 1994 for instruments descriptions) and optical thickness derived from MCR (Multi-Channel Radiometer, Rawlins and Foot 1990) reflectance measurements were used to calculate expected track contrast and contrast susceptibility for three identified tracks on 13 June and 28 June 1994. Results of these calculations are plotted in Fig. 12 with the name of the ships indicated (the *Sanko Peace*, *Safeguard*, and *Hanjin Barcelona*). Standard deviations for the calculations were derived from measured standard deviations based on flight legs of about 40km to 80km in length in the background cloud, and 6km to 80km in the tracks. Average values for the MAS retrievals of Fig. 11 are also shown.

A nice correlation exists between the relative change in the 3.7μm reflectance and the background cloud's contrast susceptibility when using average results from the combined data sets of Fig. 11. The correlation

suggests that reasonable predictions for track contrast could have been made in these instances from knowledge of background cloud microphysics (i.e., contrast susceptibility) alone without regard to actual changes in cloud droplet numbers or the dynamics of the track formation. However, AVHRR results shows much scatter which could indicate problems with pixel sampling, incompletely cloud-filled pixels, or that the increased number of tracks analyzed in the AVHRR sample gives a truer indication of track variability.

5. Summary

The relative increase in ship track reflectance, compared to background cloud reflectance values, is a measure of the track contrast. The derivative of contrast with respect to droplet concentration is a modified form of the cloud susceptibility parameter (Twomey 1991) and has been termed the *contrast susceptibility*. This sensitivity parameter increases with droplet absorption on account of cloud reflectance increases due to single scattering albedo increases dominating the effects of accompanying changes in cloud optical thickness. The 3.7μm band has the largest sensitivity to droplet numbers among the typical channels used for cloud remote sensing and is expected to have a factor of two to six times greater sensitivity than visible bands.

Both MAS and AVHRR retrievals show great variability in both background cloud and ship track optical thickness and droplet effective radius. As a generalization of the retrieval results: effective radius reduction was the most apparent signature of ship tracks, optical thickness changes in tracks were not much larger on average than background variability, and liquid water path seemed to decrease in tracks more often than not.

Correlations between the 3.7μm track contrast and the background cloud 3.7μm contrast susceptibility are reasonably good for MAS retrievals and C130 in situ measurements (Fig. 12). If this observed correlation is generally true, estimates of potential ship track formation from background cloud microphysics would be possible without needed details of ship effluent, droplet nucleation, and dynamic processes. However, AVHRR retrievals show much scatter and poorer correlation. This paper has focused on stratocumulus clouds in which ship tracks were readily observed. Less attention has been given to the significance and use of cloud susceptibility on days when no tracks form. Coakley et al. (1996) discuss this issue in greater detail.

Acknowledgments. D. Babb, D. P. Kratz, G. T. Arnold, M. Fitzgerald, P. Grant, J. S. Myers, and L. E. Gumley.

References

Bohren, C. F., 1980: Multiple scattering of light and some of its observable consequences. *Am. J. Phys.*, 55, 524-533.

Charlson, R. J., S. E. Schwartz, J. M. Hales, R. D. Cess, J. A. Coakley, J. E. Hansen, and D. J. Hofmann, 1992: Climate forcing by anthropogenic aerosols. *Science*, 255, 423-430.

Conover, J. H., 1966: Anomalous cloud lines. *J. Atmos. Sci.*, 23, 778-785.

Conover, J. H., 1969: New observations on anomalous cloud lines. *J. Atmos. Sci.*, 26, 1153-1154.

Coakley, J. A., R. L. Bernstein, and P. A. Durkee, 1987: Effect of ship-stack effluents on cloud reflectivity. *Science*, 237, 1020-1022.

Coakley, J. A., et al. 1996: this volume.

Ferek, R. J., et al. 1996: this volume.

Garrett, T. J., and P. V. Hobbs, 1995: Long-range transport of continental aerosols over the Atlantic Ocean and their effects on cloud structure. *J. Atmos. Sci.*, 52, 2977-2984.

Han, Q., W. Rossow, R. Welch, A. White, and J. Chou, 1995: Validation of satellite retrievals of cloud microphysics and liquid water path using observations from FIRE. J. Atmos. Sci., 52, 4183-4195.

King, M. D., W. P. Menzel, P. S. Grant, J. S. Myers, G. T. Arnold, S. E. Platnick, L. E. Gumley, S. C. Tsay, C. C. Moeller, M. Fitzgerald, K. S. Brown and F. G. Osterwisch, 1996: Airborne scanning spectrometer for remote sensing of cloud, aerosol, water vapor and surface properties. *J.Atmos. Oceanic Technol.*, 13, 777-794.

Knollenberg, R. G., 1981: Techniques for probing cloud microstructure.

Clouds: their formation, optical properties, and effects, P. V. Hobbs and A. Deepak, Eds., Academic Press, 15-91.

Kratz, D. P., 1995: The correlated k-distribution technique as applied to the AVHRR channels. *J. Quant. Spectrosc. Radiat. Transfer*, 53, 501-517.

Martin, G.M., D. W. Johnson, and A. Spice, 1994: The measurement and parametrisation of the effective radius of warm stratocumulus clouds. *J. Atmos. Sci.*, 51, 1823-1842.

Noonkester, V. R., 1984: Droplet spectra observed in marine stratus cloud layers. *J. Atmos. Sci.*, 41, 829-845.

Platnick, S., and S. Twomey, 1994: Determining the susceptibility of cloud albedo to changes in droplet concentration with the Advanced Very High Resolution Radiometer. *J. Appl. Met.*, 33, 334-347.

Platnick, S., and F. P. J. Valero, 1995: A validation of a satellite cloud retrieval during ASTEX. *J. Atmos. Sci.*, 52, 2985-3001.

Radke, L. F., J. A. Coakley, M. D. King, 1989: Direct and remote sensing observations of the effects of ships on clouds. *Science*, 246, 1146-1149.

Rawlins, F. and J. S. Foot, 1990: Remotely sensed measurements of stratocumulus properties during FIRE using the C130 aircraft multichannel radiometer. *J. Atmos. Sci.*, 47, 2488-2503.

Scorer, R. S., 1987: Ship trails. *Atmos. Environ.*, 21, 1417-1425.

Spinhirne, J. D., and T. Nakajima, 1994: The glory of clouds in the near infrared. *Appl. Opt.*, 33, 4652.

Stephens, G. L., and S. Tsay, 1990: On the cloud absorption anomaly. *Q. J. R. Meteorol. Soc.*, 116, 671-704.

Taylor, J. P., and A. McHaffie, 1994: Measurements of cloud susceptibility. *J. Atmos. Sci.*, 51, 1298-1306.

Twomey, S., H. Jacobowitz, and H. B. Howell, 1966: Matrix methods for multiple scattering problems. *J. Atmos. Sci.*, 23, 101-108.

Twomey, S., H. B. Howell, and T. A. Wojciechowski, 1968: Comments on anomalous cloud lines. *J. Atmos. Sci.*, 26, 1272-1282.

Twomey, S., 1974: Pollution and the planetary albedo. *Atmos. Environ.*, 8, 1251-1256.

Twomey, S., 1977: The influence of pollution on the shortwave albedo of clouds. *J. Atmos. Sci.*, 34, 1149-1152.

Twomey, S., and C. F. Bohren, 1980: Simple approximations for calculations of absorption in clouds. *J. Atmos. Sci.*, 37, 2086-2094.

Twomey, S., 1991: Aerosols, clouds and radiation. *Atmos. Environ.*, 254, 2435-2442.

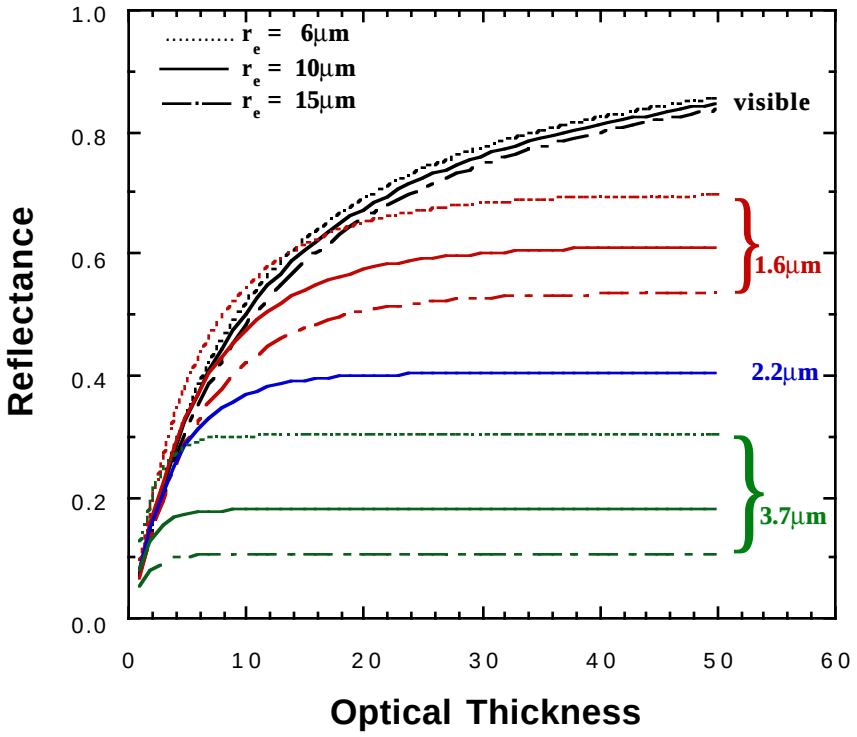

Fig. 1 Plots of bidirectional reflectance versus optical thickness for the MODIS Airborne Simulator channels with central wavelengths at 0.65μm, 1.62μm, 2.13μm, and 3.74μm. Reflectance for each channel is shown for effective radii of 6μm, 10μm, and 15μm (or only a 10μm radius for the 2.13μm channel). Calculations are averaged over the azimuth where the cosine of the solar and satellite viewing angles are 0.65 and 0.85, respectively. Optical thickness is the visible equivalent.

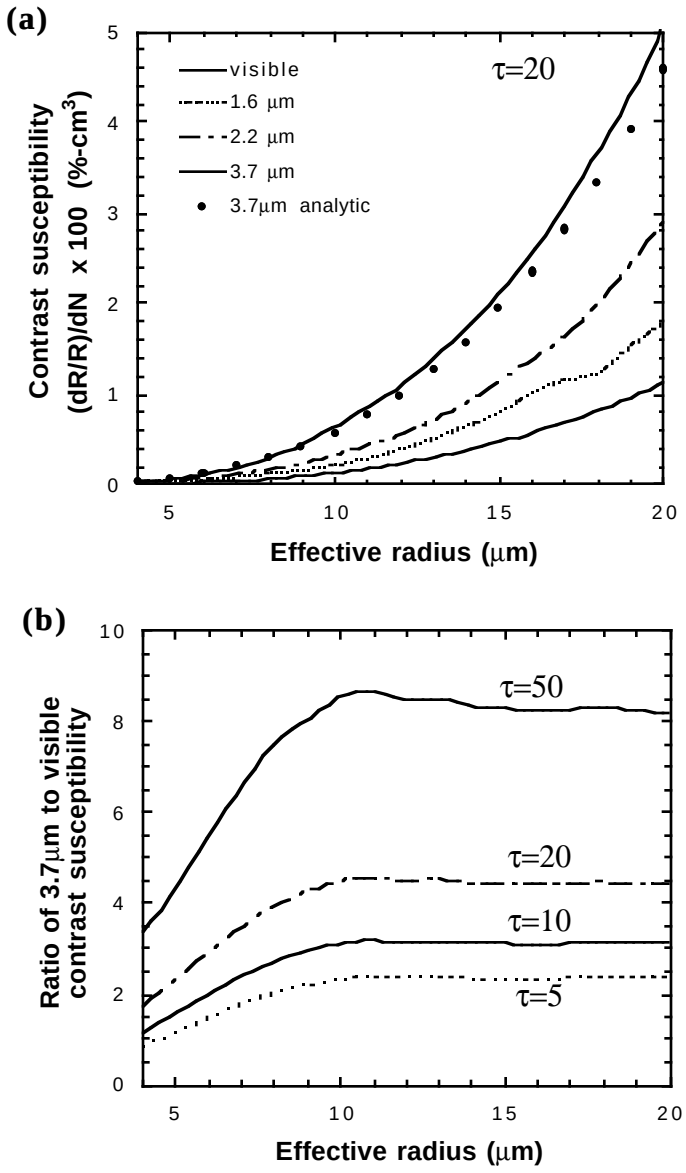

Fig. 2 (a) The contrast, or relative, susceptibility calculated in visible and near-infrared bands as a function of cloud droplet effective radius for an optical thickness of 20. An analytic approximation for the 3.7μm curve is also shown (see text). (b) Ratios of the 3.7μm contrast susceptibility to the visible for a wide range of optical thicknesses. Solar and viewing geometries are the same as in Fig. 1, liquid water content is 0.3 gm^{-3}.

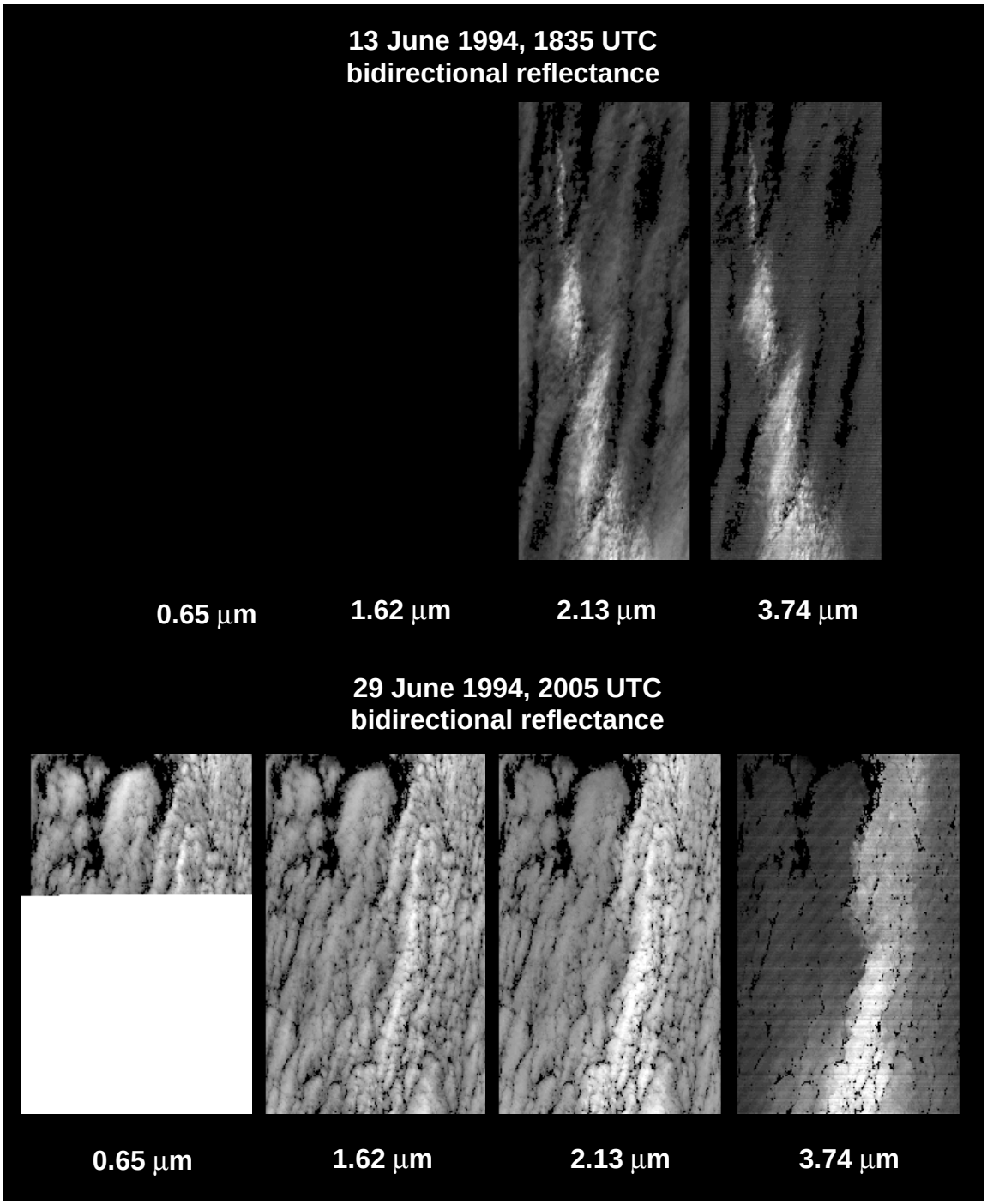

Fig. 3 Cloud reflectance in four visible and near-infrared MODIS Airborne Simulator channels showing the general increase in ship track contrast at the longer wavelengths. Model calculations suggest that at the relatively high sun angles present during these flights, the 3.7μm track contrast would be about a factor of 1.6 greater than in the visible; larger contrast differences would be expected at lower sun angles. Emission has been removed from the 3.7μm channel.

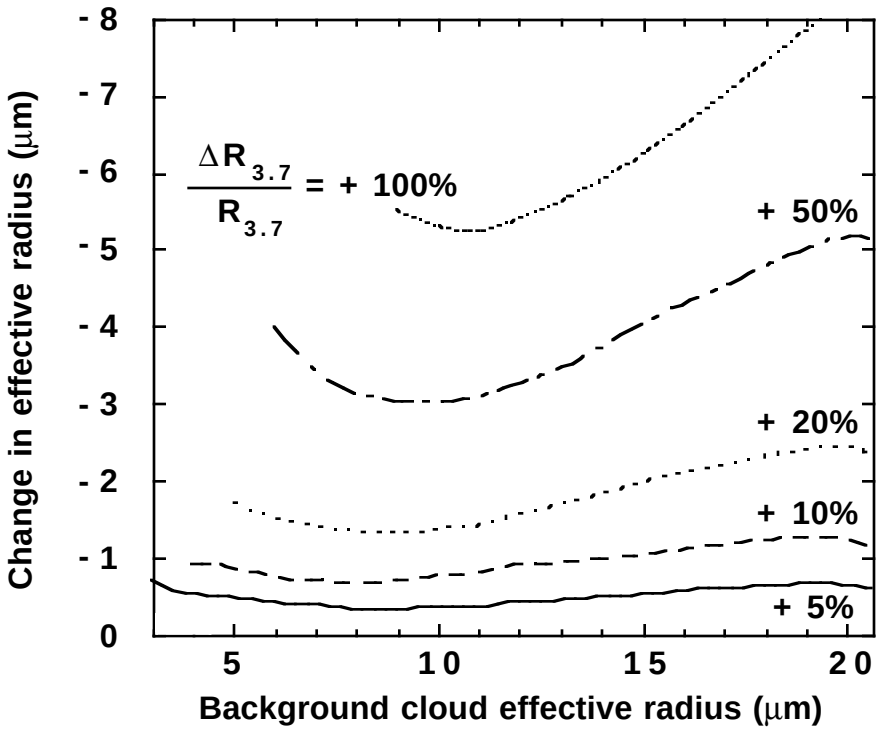

Fig. 4 Curves showing the relative change in 3.7μm cloud reflectance expected for a given reduction in droplet size occuring in a ship track relative to the background cloud in which it forms. Solar and viewing geometries are the same as in Fig. 1, liquid water content is 0.3 gm^{-3}.

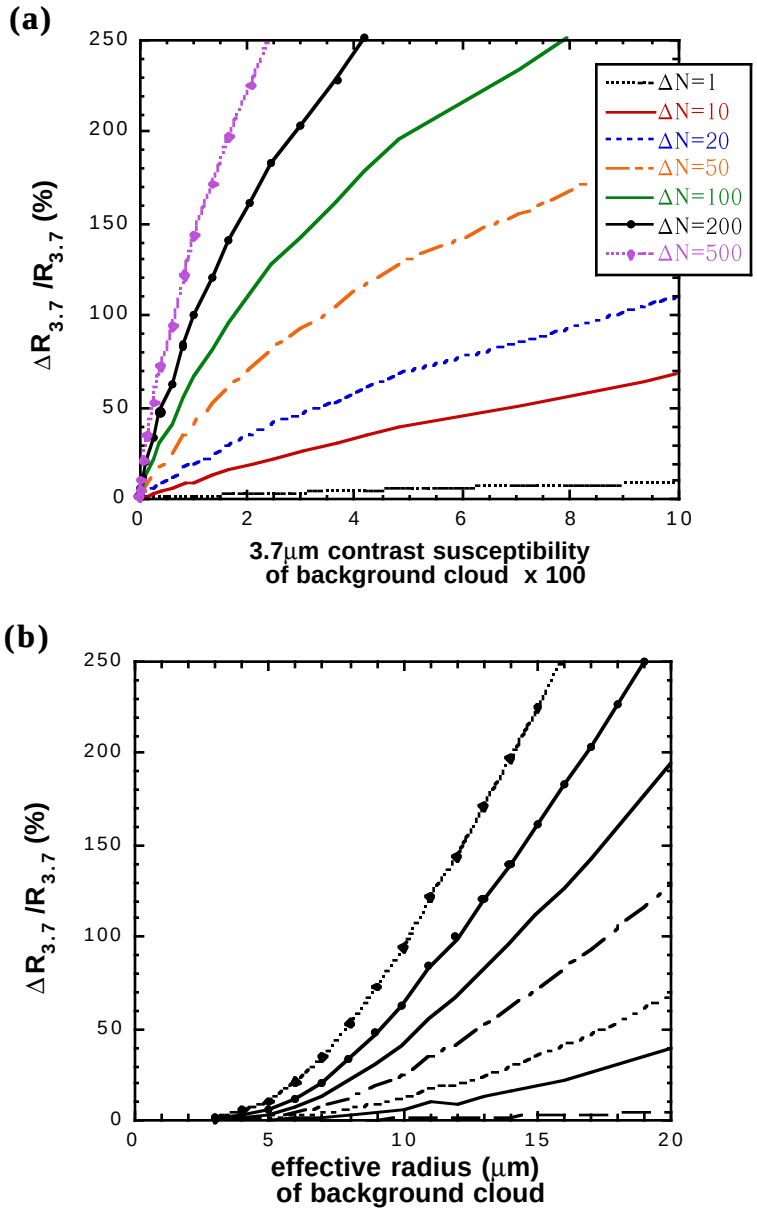

Fig. 5 (a) Calculations showing the ship track contrast in the 3.7μm band versus the contrast susceptibility of the background cloud for a wide range of droplet concentration increases. Calculated for a liquid water content of 0.3gm^{-3}, an optical thickness of 10, and with solar and viewing angles the same as for Fig. 1. (b) The same as in (a) but with the abscissa transformed to effective radius.

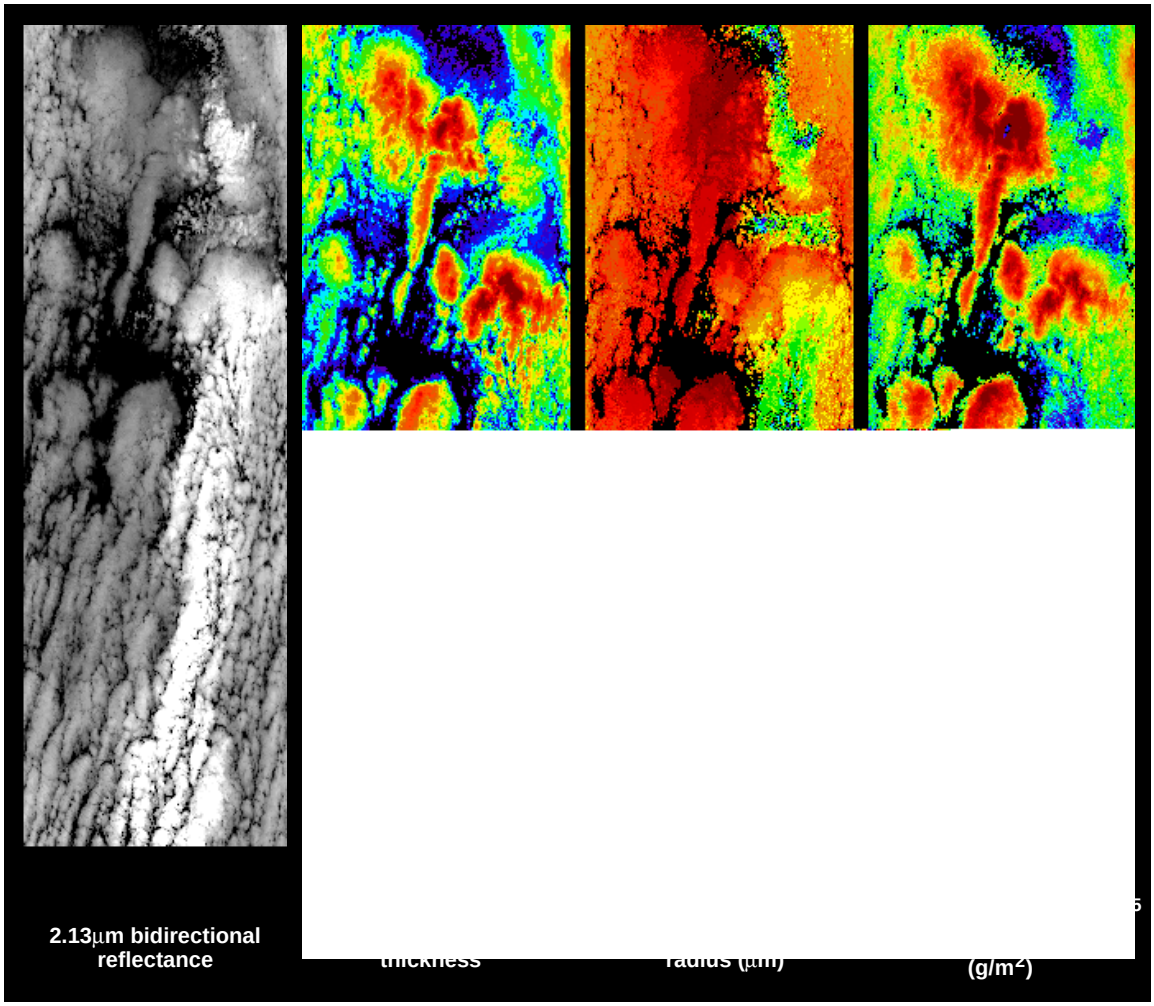

Fig. 6 Cloud reflectance and retrievals for the sourthern portion of the Star Livorno ship track (center of images at 35.95N, 125.45W) on 29 June 1994, 2000 UTC, using the MODIS Airborne Simulator visible and 2.13μm channels.

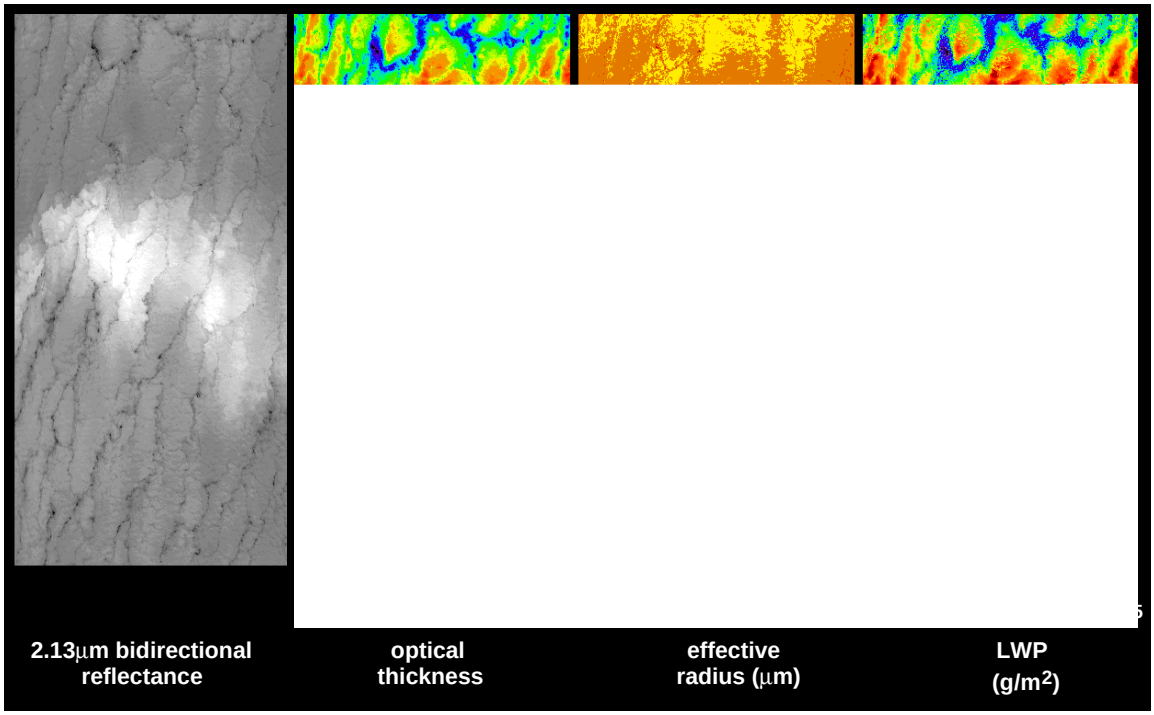

Fig. 7 Cloud reflectance and retrievals of a ship track on 30 June 1994, 2015 UTC, using the MODIS Airborne Simulator visible and 2.13μm channels. Center of images located at 35.36N, 125.13W.

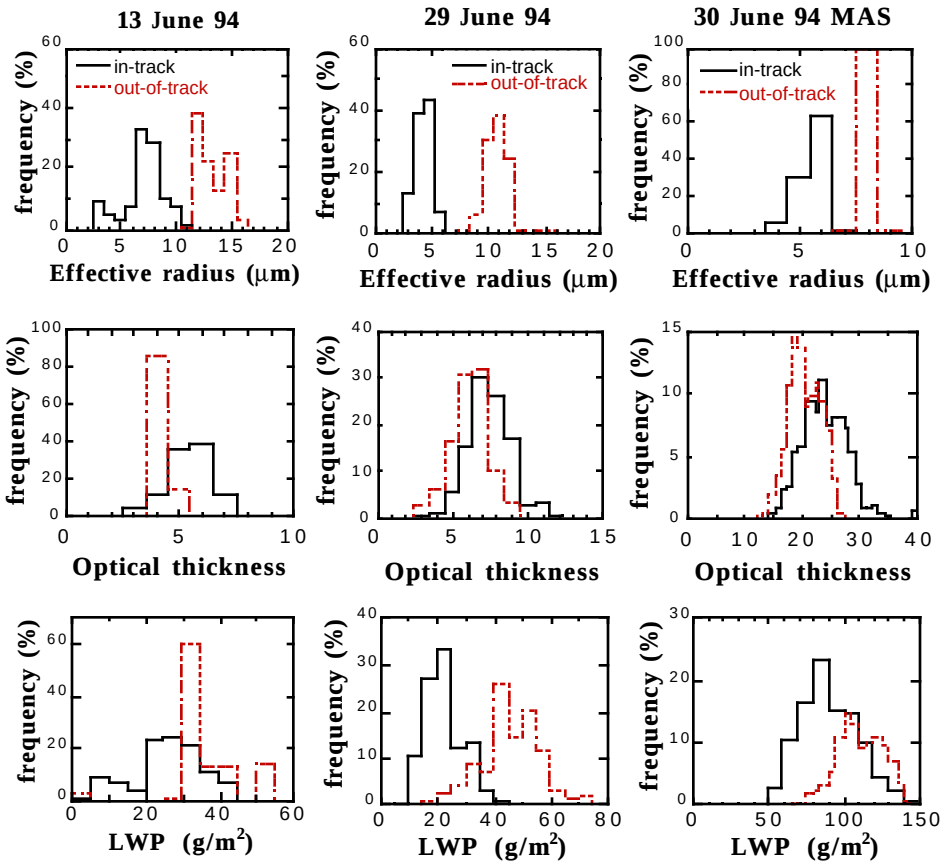

Fig. 8 Selected histograms of cloud retrievals using the MODIS Airborne Simulator visible and 2.13μm channels, for three tracks on three different days. Retrievals are for selected track and nearby background cloud locations. Because of the large variability in both in-track and background cloud parameters, there is no unique histogram for any of the tracks.

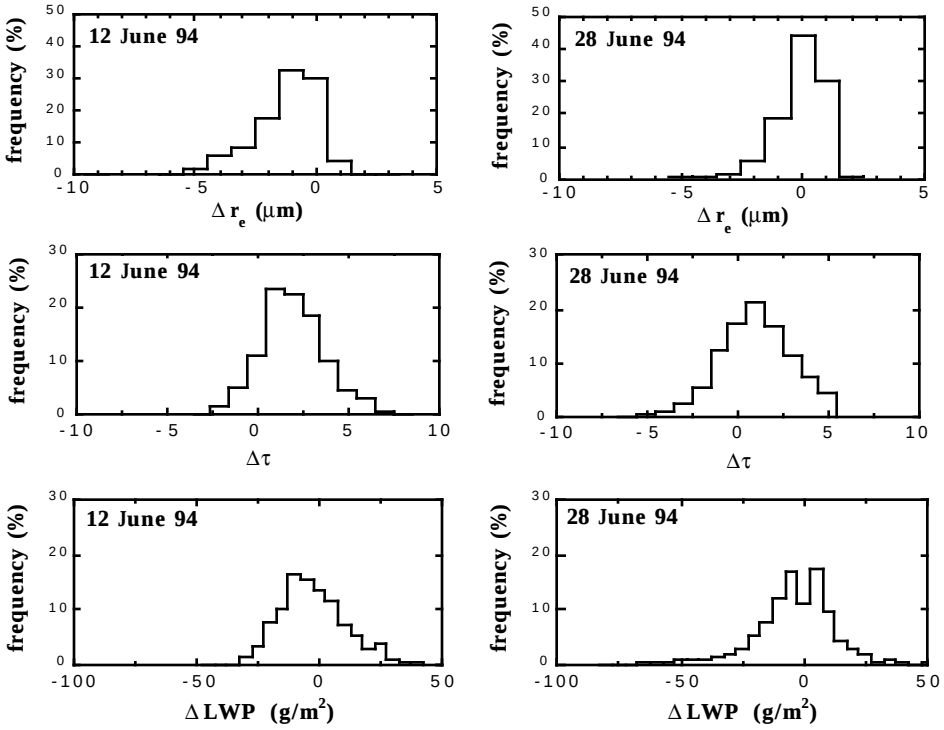

Fig. 9 Histograms of *changes* in AVHRR cloud retrievals for 12 June and 28 June 1994, calculated for numerous pairs of track and nearby background cloud locations.

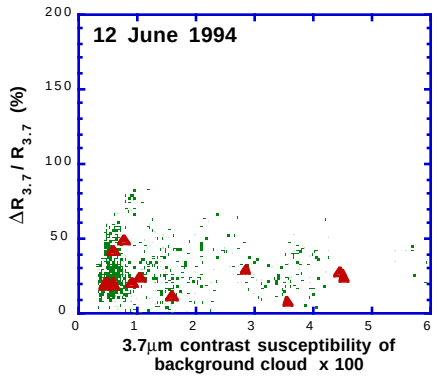
12 June 1994
ΔR3.7 / R3.7 (%)
3.7μm contrast susceptibility of
background cloud x 100

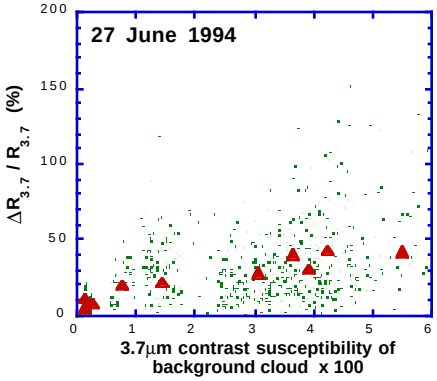
27 June 1994
ΔR3.7 / R3.7 (%)
3.7μm contrast susceptibility of
background cloud x 100

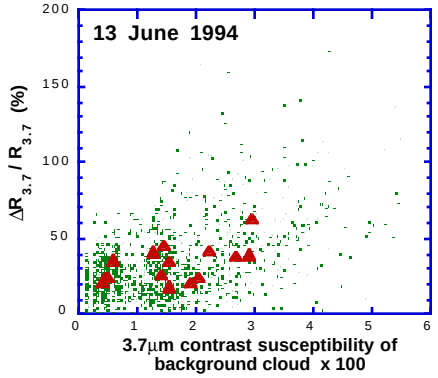
13 June 1994
ΔR3.7 / R3.7 (%)
3.7μm contrast susceptibility of
background cloud x 100

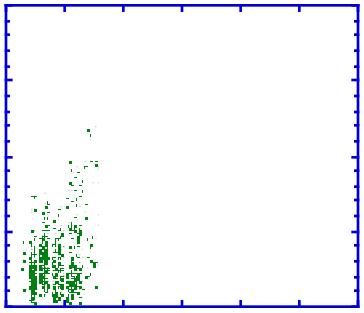

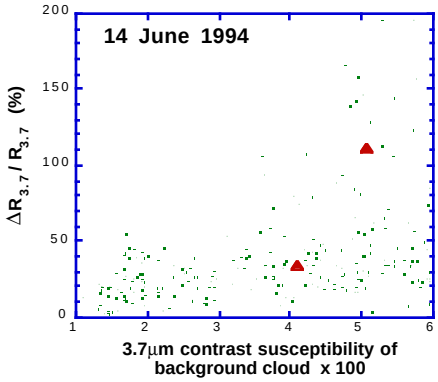
14 June 1994
ΔR3.7 / R3.7 (%)
3.7μm contrast susceptibility of
background cloud x 100

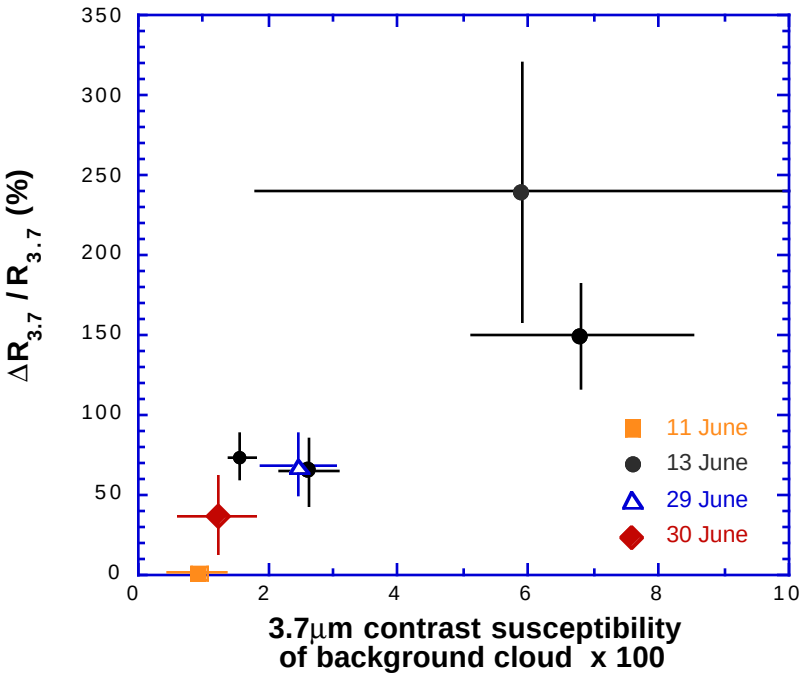

Fig. 11 Plot of the measured relative change in the MODIS Airborne Simulator (MAS) 3.7μm channel reflectance versus the 3.7μm contrast susceptibility of the background cloud on four different days. Each symbol respresents the averages for a single track (excetp 11 June when no tracks were observed) while bars represent the standard deviations.

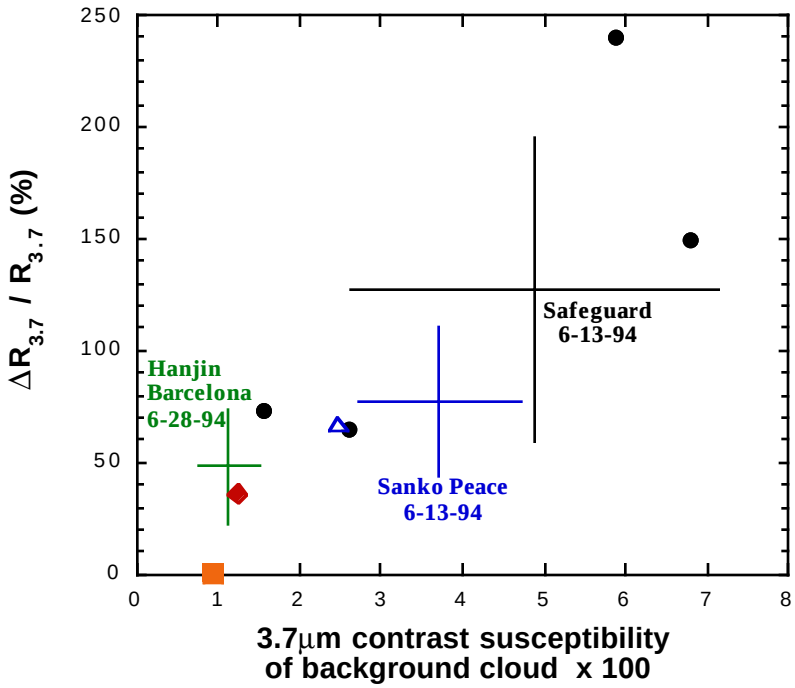

Fig. 12 Plot of the calculated relative change in a 3.7μm channel reflectance versus the 3.7μm contrast susceptibility of the background cloud for three ship tracks. Calculations based on in situ droplet size and above-cloud reflectance measurements of optical thickness made by the UK Meteorological Research Flight C130 aircraft; bars represent the standard deviations. Averaged values for the MAS/ER-2 tracks of Fig. 11, with the same symbol definitions, are also shown.